Physicochemical origin of improvement of magnetic and transport properties of STT-MRAM cells using Tungsten on FeCoB storage layer

Jyotirmoy Chatterjee, Eric Gautier, Marc Veillerot, Ricardo Sousa, Stéphane Auffret, Bernard Dieny

Physicochemical origin of improvement of magnetic and transport properties of STT-MRAM cells using Tungsten on FeCoB storage layer

Jyotirmoy Chatterjee[1*], Eric Gautier[1], Marc Veillerot[2], Ricardo C. Sousa[1], Stéphane Auffret[1] and Bernard Dieny[1]

1) Univ. Grenoble Alpes, CEA, CNRS, Grenoble-INP, INAC-SPINTEC, Grenoble, France

2) Univ. Grenoble Alpes, CEA-LETI, Minatec Campus, Grenoble, France

Abstract

We investigated and compared the structural and magnetic properties of MgO/FeCoB based out-of-plane magnetized tunnel junctions at thin film level as well as the magneto-transport properties of corresponding patterned STT-MRAM cells comprising either Ta 1 nm or W2 /Ta1 nm cap layers for different annealing temperatures up to 455°C. W material in the cap was found to improve the structural stiffness of the perpendicular magnetic tunnel junctions and most importantly prohibits Fe diffusion from the FeCoB storage layer to the cap layer, remarkably improving the thermal robustness and magneto-transport properties of the stacks and of the corresponding patterned memory cells. As a result, the interfacial anisotropy constant of the MgO/FeCoB interfaces is improved by 17-29% compared to Ta cap. The STT-MRAM cells fabricated from the pMTJ stacks with W/Ta cap reveal a significant improvement of tunneling magnetoresistance and thermal stability factor, which are respectively 120% and 52 as compared to 70% and 35 for the stack with Ta cap. This improvements are ascribed to the enhancement of MgO crystallinity upon higher temperature annealing (425°C) as well as prohibition Fe out-diffusion.

*Present address: University of California, Berkeley

Perpendicular spin transfer torque random access memory (pSTT-MRAM) based on perpendicular magnetic tunnel junction (pMTJ) stack has attracted considerable interest due to their combination of assets of non-volatility, high thermal stability, low critical current for current-induced spin transfer torque (STT) magnetization switching (few tens of microamps at sub-40nm), high speed (write access time typically in the range 10ns-30ns) and high density memory array (4Gbit capacity and 1.5F pitch demonstrated).[1–6] The core component of the stack, where spin transport phenomena such as tunneling magnetoresistance (TMR) and magnetization reversal of storage layer by STT occurs is an FeCoB/MgO/FeCoB based tunnel junction.[7–9] Here one of the FeCoB layer is storage layer, while other has a fixed magnetization, called as reference layer. The reference layer is commonly pinned by exchange interaction with Co/Pt or Co/Pd based synthetic antiferromagnet (SAF).[10,11] The perpendicular magnetic anisotropy (PMA) required to provide a long enough retention of the memory cell originates from the MgO/FeCoB interface due to Fe-O orbitals hybridization.[12–14] However, a cap layer used on top of storage layer, can also indirectly influence the magnetic and transport properties of the pMTJ by modifying the interfacial and bulk physicochemical and electronic properties.[15–18] The main physicochemical modifications are Boron absorption from the storage layer[17] or interdiffusion during sputtering or post deposition anneals.[15] In an earlier paper, we reported significant improvement of annealing tolerance using thick W/Ta cap as compared to Ta because of structural stiffening of the stack and much weaker interdiffusion with W than with Ta. In this report, we show that the interfacial PMA of MgO/FeCoB interface with W2/Ta1 nm cap is larger than with Ta 1nm cap after annealing at all investigated annealing temperatures (315°C-455°C) and explain the physicochemical reasons behind this improvement. In addition, we investigated the magneto-transport properties of sub-100nm diameter memory cells fabricated from pMTJ stacks with these two different cap layers and with different annealing up to 425°C. Note that this annealing temperature is higher than back-

end-of-line (BEOL) process temperature. A significant improvement in TMR (from 70% up to 120%) and thermal stability factor (Δ) (from 35 up to 52) is reported for 80 nm devices when a Ta cap layer is replaced by a W/Ta cap.

The samples were deposited on Si wafer by magnetron sputtering under an Ar pressure of 2×10^{-3} mbar. The MgO tunnel barrier was obtained by naturally oxidizing a metallic Mg layer under an oxygen pressure of 3×10^{-2} mbar with a flow rate of 100 sccm. On top of this oxidized layer, a second Mg layer 0.5 nm thick was deposited. All the samples were annealed for 10 min at different temperatures under high vacuum (5×10^{-6} mbar). The effective perpendicular anisotropy was calculated from the area between perpendicular and in-plane M(H) loops measured by vibrating sample magnetometer (VSM). At first, the magnetic parameters, such as magnetic dead layer thickness (t_d), saturation magnetization (M_s) and interfacial anisotropy constant (K_i) of the storage electrodes consisting of *Ta 3/FeCoB 0.4/Mg 0.8/Oxidation 30s/Mg 0.5/FeCoB 1.2/cap/Pt 3nm* were derived as a function of annealing temperature and are listed in table 1. The values of M_s and t_d were calculated from the slope and x-intercept of the *m/A* (magnetic moment per unit area) versus *t* plots, where *t* is the nominal thickness determined from the deposition rate. The dead layer thicknesses are observed to be similar for both caps. However, the values of M_s of FeCoB at annealing temperatures ≥ 400 °C are higher for W/Ta than with Ta cap. Interfacial anisotropy constants (K_i) were evaluated from the y-intercepts after fitting the linear zone of $K_{eff}.(t-t_d)$ vs. $(t-t_d)$ graphs using the equation

$$K_{eff} = \frac{K_i}{t - t_d} - 2\pi {M_s}^2 \qquad (1)$$

Figure 1 shows $K_{eff}.(t-t_d)$ vs. $(t-t_d)$ graphs at various annealing stages for W/Ta and Ta caps. K_i for W/Ta cap is 1.05 erg/cm^2, which is about 24% higher than that of Ta cap.

At this point, a question is raised, why W in cap layer yields higher interfacial anisotropy? In order to understand the reason of interfacial anisotropy enhancement for storage layer caped with W instead of Ta, chemical profiling with dynamic secondary ion mass spectroscopy (DSIMS) were carried out for two stacks with simpler structure *Si/ Mg 0.7/Oxidation/Mg 0.5/FeCoB 1.6/(W2 or Ta2)/Pt 3 nm*. We discuss the comparisons between the SIMS profiles for Ta and W caps depicted in Fig. 2, focusing in particular at the MgO top interface, as this interface plays a determinant role in the PMA amplitude. Note that, the MgO-barrier/FeCoB interface is nominally identical in both structures. However, the comparisons of the Fe elemental profiles with Ta cap (Fig. 2a) and with W cap (Fig. 2d) in the as-deposited samples already reveal a clear difference between the two samples. In the sample with Ta cap, an enrichment of Fe content is observed next to the Ta interface. A pronounced peak of Fe concentration is indeed observed next to this interface and a weaker one next to the MgO interface implying preferred Fe migration towards the Ta cap during deposition. In contrast, in the sample with W cap, the Fe concentration is higher next to the MgO interface as shown in Fig. 2d. In the annealed sample with Ta cap, the Fe concentration enhancement near the Ta interface is even more pronounced (see Fig. 2b,c) indicating that Fe has even more migrated towards this interface while the Fe content next to the MgO interface has decreased. On the other hand, for the annealed sample with W cap, the Fe concentration tends to become more uniform over the whole FeCoB layer as obvious from Fig 2(e,f). The significant migration of Fe towards the capping layer in the sample with Ta cap and its prohibition in the sample with W cap is ascribed to the much larger negative enthalpy of formation of FeTa (-3468 meV/atom) than of FeW (-554 meV/atom).[19] Comparatively, the enthalpy of formation of CoTa (-253meV/atom) and CoW(-84meV/atom) are relatively weak which explains the absence of significant Co migration towards the cap layer. As a result of using W cap, a higher Fe concentration along the MgO interface can be maintained upon annealing than in the case of

Ta cap. Therefore, larger interfacial anisotropy with W cap than with Ta cap is produced as the interfacial anisotropy at Fe/MgO interface is larger than at Co/MgO interface.[13,14] As a consequence, the effective magnetic critical thicknesses (t_c), listed in table 1, above which the FeCoB layer becomes in-plane magnetized are higher for W cap than for Ta cap. In addition to Fe, there is also a significant difference in B profile between the two caps observed from the SIMS profile. Both ass deposited samples have higher Boron concentration near the MgO interface as well as near the interface with cap layer. The peak near MgO suggests formation of B-oxides, which is in agreement with previous reports.[15,17] Although both cap layers absorb B out from the FeCoB layer upon annealing, Ta serves as a better B getter than W due to the decreasing absolute value of enthalpy of formation of metal borides along the series (Hf, Ta, W, Re, Os) .[20] It is clear from the figure that for both caps, Boron is not completely absorbed by the cap layer. After annealing at 400°C or 450°C, some Boron still remains along the MgO interface. For W cap, higher amount of B seems to be left over near the MgO interface as compared to the Ta cap case. Nevertheless, W cap yields higher PMA suggesting that the prohibition of preferential Fe migration with W cap is the dominant mechanism.

After having focused on the magnetic properties of the top electrode storage layer and investigated the role of W in the cap layer, pMTJ stacks using Ta 1nm and W2/Ta 1nm caps were patterned to characterize the magneto-electric properties of memory cells as a function of annealing temperature. For this purpose, three samples were deposited on 100 mm Si wafers. One pMTJ with Ta 1nm cap, annealed at 340 °C and the other two with W2/Ta1 nm annealed at 400 °C and 425 °C for 30mins. The layer configurations of these pMTJ stacks was *Si/bottom electrode/Pt 5/(Co/Pt) ML based SAF/Ta 0.3/FeCoB 1.2/Mg-wedge/Oxidation-240s/Mg 0.5/FeCoB-wedge/cap (Ta 1/Pt 3* or *W 2/Ta 1/Pt 3 nm).* One must note that the directions of wedges are orthogonal to each other. The SAF layer consists of hard layer (HL: *[Co 0.5/Pt 0.25]$_6$/Co 0.5 nm*) and reference layer (RL: *[Co 0.5/Pt 0.25]$_3$/Co 0.5/Ta 0.3/FeCoB 1.2 nm*)

antiferromagnetically coupled by 0.9 nm Ru layer.[16,21] Co/Pt MLs based SAF are widely used in the pMTJ stacks[22,23] because of their large PMA[24–26], which makes them good candidates for realizing magnetically hard layers.

TMR versus FeCoB thicknesses for the three samples are shown in Fig. 3. TMR increases as a function of FeCoB thickness due to the improvement of the crystalline quality of the FeCoB layer and to the reduced amount of thermal fluctuations at room temperature in thicker magnetic layer. Above the critical thickness, TMR reduces again as the PMA of the storage layer decreases and correlatively the degree of magnetic antiparallel alignment between storage layer and reference layer. For W/Ta cap, the maximum TMR (120%) is larger than the one with Ta cap (70%). Moreover, the stack with W/Ta after annealing 425°C yields the highest TMR (120%) since both the storage layer and the MgO barrier then exhibit the best crystallinity among the three wafers thanks to the high temperature annealing.[27]

High-resolution transmission electron microscopy imaging of pMTJ stacks were performed to investigate the crystallinity upon annealing at 340°C and 425°C, which are shown in Fig. 4(a) and (b) respectively. An improved MgO crystallinity after annealing at 425°C as compared with 340°C annealing can be observed, which is the one of the possible reasons of obtaining larger TMR for W cap. Moreover, the reduced Fe out-diffusion when using W cap likely improves the spin-polarization of Δ_1 tunneling states resulting in higher TMR than with Ta cap. This is in agreement with the report of F. Bonell et al. where they demonstrated that TMR decreases for higher Co content in FeCo, due to onset of minority Δ_1 states at Fermi energy.[28] Lastly, ab initio calculations of FeCo/MgO/FeCo tunnel junctions with different cap layers also demonstrated increased TMR with W cap compared with Ta due to the improvement of spin-polarization of Δ_1 tunneling states.[29]

The W cap layer on storage layer shows nanocrystalline or even amorphous structure (see Fig. 4). In our previous work[16], the improvement of thermal tolerance was explained in terms

of overall improvement of the mechanical stiffness due to the incorporation of W as its melting temperature is very high, 3422°C. The observation that W is nanocrystalline or even amorphous further supports this explanation ruling out the possibility of crystallinity of W being responsible for high thermal tolerance as stated before by G. An et al.[30]

The thermal stability factors of patterned memory cells were calculated from statistical measurements of resistance versus magnetic field (R(H)) loops using the switching field distribution model.[31,32] According to this model, the thermal stability factor Δ can be derived by fitting the switching probability of the cells using the equation below :

$$P_{sw}(H) = 1 - \exp[-\frac{f_0 H_k}{2r}\sqrt{\frac{\pi}{\Delta}}erfc\left\{\sqrt{\Delta}(1-\frac{H}{H_k})\right\}] \qquad (2)$$

In this equation f_0, r and H_k are the attempt frequency (1 GHz), field sweep rate (typically 40 kOe/s) and anisotropy field respectively. For each memory cells, 300 R(H) loops were measured. Then the probability of switching was calculated and fitted with the equation to extract Δ. Following this method, Δ of 80 nm patterned cells were calculated and plotted as a function of effective storage layer thickness in Fig. 5. The sample with Ta 1 nm cap layer shows an average Δ about 35 at the effective thickness of 0.85 nm, where the maximum TMR was obtained. For the samples with W2/Ta1 nm cap, the average value of Δ obtained is 52 at the effective thickness 0.95 nm (shown in Fig. 5 (b) and (c)), which is about 50% higher than in the sample with Ta cap. One must note that the error bars are large due to process variation and selection of 80 nm cells with Mg wedge thickness in the range of 1.5 Å. The thermal stability factor increases as a function of thickness, which can be fitted assuming the energy barrier of magnetization reversal as $E_B = K_{eff}V_n$ where, K_{eff} is effective perpendicular anisotropy of storage layer and V_n is the nucleation volume. The nucleation diameter is comparable to the domain wall width (δ_w) and therefore, Δ can be expressed by the equation below.[33]

$$\Delta = \frac{E_B}{k_B T} = K_{eff}\pi\left(\frac{\delta_w}{2}\right)^2 t = K_{eff}\pi\left(\frac{\pi}{2}\sqrt{\frac{A_{ex}}{K_{eff}}}\right)^2 t = \frac{\pi^3 A_{ex} t}{4} \qquad (3)$$

Using this equation Δ vs. FeCoB thickness (t) plots were fitted and the exchange stiffness constant (A_{ex}) was calculated from the slope. The calculated values of A_{ex} are 29.3 and 26.6 pJ/m after 400°C and 425°C annealing respectively, which are close to the values reported by Yamnouchi et al.[34]

In summary, we demonstrated that W on top of FeCoB prohibits Fe out-diffusion, which occurs in case of Ta cap. The resulting interfacial compositional integrity yields a 17-29 % higher interfacial anisotropy of the storage layer with W2/Ta1 nm cap than with Ta 1 nm cap. Transport properties of 80 nm memory cells also exhibit 50 % enhancement in thermal stability factor (Δ) as well as a significant improvement in TMR (70% for Ta cap, 120% for W/Ta) with W/Ta cap compared with Ta cap. This improvement is attributed to the higher Fe concentration at the interface with MgO as well as improvement of crystallinity of the tunnel junction upon high temperature annealing up to 425°C, which is higher than BEOL thermal budget. By fitting the variation of Δ vs. effective FeCoB thickness, the exchange stiffness constants (A_{ex}) of FeCoB with W/Ta cap were evaluated to be 29.3 and 26.6 pJ/m after 400°C and 425°C annealing respectively.

Acknowledgement

This work was funded under the ERC Adv grant MAGICAL N° 669204 and J.C. acknowledges LabEx Minos ANR-10-LABX-55–01 for fellowship.

Bibliography

[1] S. Mangin, D. Ravelosona, J.A. Katine, and E.E. Fullerton, Nat. Mater. **5**, 210 (2006).

[2] T. Kishi, H. Yoda, T. Kai, T. Nagase, E. Kitagawa, M. Yoshikawa, K. Nishiyama, T. Daibou, M. Nagamine, M. Amano, S. Takahashi, M. Nakayama, N. Shimomura, H. Aikawa, S. Ikegawa, S. Yuasa, K. Yakushiji, H. Kubota, a. Fukushima, M. Oogane, T. Miyazaki, and K. Ando, 2008 IEEE Int. Electron Devices Meet. 1 (2008).

[3] S. Ikeda, K. Miura, H. Yamamoto, K. Mizunuma, H.D. Gan, M. Endo, S. Kanai, J. Hayakawa, F. Matsukura, and H. Ohno, Nat. Mater. **9**, 721 (2010).

[4] J.M. Slaughter, K. Nagel, R. Whig, S. Deshpande, S. Aggarwal, M. Deherrera, J. Janesky, M. Lin, H.J. Chia, M. Hossain, S. Ikegawa, F.B. Mancoff, G. Shimon, J.J. Sun, M. Tran, T. Andre, S.M. Alam, F. Poh, J.H. Lee, Y.T. Chow, Y. Jiang, H.X. Liu, C.C. Wang, S.M. Noh, T. Tahmasebi, S.K. Ye, and D. Shum, Tech. Dig. - Int. Electron Devices Meet. IEDM 21.5.1 (2016).

[5] D. Apalkov, B. Dieny, and J.M. Slaughter, Proc. IEEE **104**, 685 (2016).

[6] V.D. Nguyen, P. Sabon, J. Chatterjee, L. Tille, P. Veloso Coelho, S. Auffret, R. Sousa, L. Prejbeanu, E. Gautier, L. Vila, and B. Dieny, Tech. Dig. - Int. Electron Devices Meet. IEDM 38.5.1 (2017).

[7] W. Butler, X.-G. Zhang, T. Schulthess, and J. MacLaren, Phys. Rev. B **63**, 1 (2001).

[8] J.C. Slonczewski, J. Magn. Magn. Mater. **159**, L1 (1996).

[9] L. Berger, Phys. Rev. B **54**, 9353 (1996).

[10] J. Chatterjee, T. Tahmasebi, J. Swerts, G.S. Kar, and J. De Boeck, Appl. Phys. Express **8**, 063002 (2015).

[11] K. Mizunuma, M. Yamanouchi, S. Ikeda, H. Sato, H. Yamamoto, H.D. Gan, K. Miura, J. Hayakawa, F. Matsukura, and H. Ohno, Appl. Phys. Express **4**, 60 (2011).

[12] S. Monso, B. Rodmacq, S. Auffret, G. Casali, F. Fettar, B. Gilles, B. Dieny, and P. Boyer,

Appl. Phys. Lett. **80**, 4157 (2002).

[13] H.X. Yang, M. Chshiev, B. Dieny, J.H. Lee, A. Manchon, and K.H. Shin, Phys. Rev. B - Condens. Matter Mater. Phys. **84**, 1 (2011).

[14] B. Dieny and M. Chshiev, Rev. Mod. Phys. **89**, 025008 (2017).

[15] N. Miyakawa, D.C. Worledge, and K. Kita, Magn. Lett. IEEE **4**, 2 (2013).

[16] J. Chatterjee, R.C. Sousa, N. Perrissin, S. Auffret, C. Ducruet, and B. Dieny, Appl. Phys. Lett. **110**, 202401 (2017).

[17] S. Mukherjee, R. Knut, S.M. Mohseni, T.N. Anh Nguyen, S. Chung, Q. Tuan Le, J. Åkerman, J. Persson, A. Sahoo, A. Hazarika, B. Pal, S. Thiess, M. Gorgoi, P.S. Anil Kumar, W. Drube, O. Karis, and D.D. Sarma, Phys. Rev. B - Condens. Matter Mater. Phys. **91**, 1 (2015).

[18] S. Peng, M. Wang, H. Yang, L. Zeng, J. Nan, J. Zhou, Y. Zhang, A. Hallal, M. Chshiev, K.L. Wang, Q. Zhang, and W. Zhao, Sci. Rep. **5**, 18173 (2015).

[19] M.C. Troparevsky, J.R. Morris, P.R.C. Kent, A.R. Lupini, and G.M. Stocks, Phys. Rev. X **5**, 1 (2015).

[20] C. Colinet and J.-C. Tedenac, Crystals **5**, 562 (2015).

[21] L. Cuchet, Magnetic and Transport Properties of Single and Double Perpendicular Magnetic Tunnel Junctions, Universite Grenoble Grenoble Alpes, 2015.

[22] L. Cuchet, B. Rodmacq, S. Auffret, R.C. Sousa, and B. Dieny, Appl. Phys. Lett. **105**, 1 (2014).

[23] J. Chatterjee, T. Tahmasebi, J. Swerts, G.S. Kar, and J. De Boeck, Appl. Phys. Express **8**, (2015).

[24] G.G. D. Weller, R.F.C. Farrow, R.F. Marks, G.R. Harp, H. Notarys and IBM, in *Proc. Mater. Res. Soc. Conf. (Materials Res. Soc. 313)* (1993), pp. 791–797.

[25] J. Chatterjee, T. Tahmasebi, S. Mertens, G.S. Kar, T. Min, and J. De Boeck, IEEE Trans.

Magn. **50**, 4401704 (2014).

[26] S. Bandiera, R.C. Sousa, B. Rodmacq, and B. Dieny, Appl. Phys. Lett. **100**, 142410 (2012).

[27] S. V. Karthik, Y.K. Takahashi, T. Ohkubo, K. Hono, S. Ikeda, and H. Ohno, J. Appl. Phys. **106**, (2009).

[28] F. Bonell, T. Hauet, S. Andrieu, F. Bertran, P. Le Fèvre, L. Calmels, A. Tejeda, F. Montaigne, B. Warot-Fonrose, B. Belhadji, A. Nicolaou, and A. Taleb-Ibrahimi, Phys. Rev. Lett. **108**, 1 (2012).

[29] J. Zhou, W. Zhao, Y. Wang, S. Peng, J. Qiao, L. Su, L. Zeng, N. Lei, L. Liu, Y. Zhang, and A. Bournel, Appl. Phys. Lett. **109**, (2016).

[30] G.G. An, J. Bin Lee, S.M. Yang, J.H. Kim, W.S. Chung, and J.P. Hong, Acta Mater. **87**, 259 (2015).

[31] X. Feng and P.B. Visscher, J. Appl. Phys. **95**, 7043 (2004).

[32] L. Tillie, E. Nowak, R.C. Sousa, M.C. Cyrille, B. Delaet, T. Magis, A. Persico, J. Langer, B. Ocker, I.L. Prejbeanu, and L. Perniola, Tech. Dig. - Int. Electron Devices Meet. IEDM 27.3.1 (2016).

[33] H. Sato, M. Yamanouchi, and K. Miura, IEEE Magn. Lett. **3**, 1 (2012).

[34] M. Yamanouchi, A. Jander, P. Dhagat, S. Ikeda, F. Matsukura, and H. Ohno, IEEE Magn. Lett. **2**, 3000304 (2011).

Annealing temperature (°C)	Ta 1nm cap				W2/Ta1 nm cap			
	M_s (emu/cm^3)	t_d (Å)	t_c (Å)	K_i (erg/cm^2)	M_s (emu/cm^3)	t_d (Å)	t_c (Å)	K_i (erg/cm^2)
315	1216±26	5.5	9.6	0.78±0.02		-	-	-
340	1262±14	5.6	9.6	0.87±0.03	1210±26	5.5	10.5	1.02±0.037
400	1252±54	6.1	8.1	0.85±0.025	1368±49	6.25	9.4	1.06±0.028
425	-	-			1340±50	6.2	9.4	1.05±0.034
455	-	-			1375±41	6.5	9.4	1.13±0.038

Table 1: Saturation magnetization (M_s), dead layer thickness (t_d), effective magnetic critical thickness *(t_c) and interfacial anisotropy constant (K_i) of FeCoB storage electrode with Ta 1 and W2/Ta1 nm cap at various annealing temperatures.*

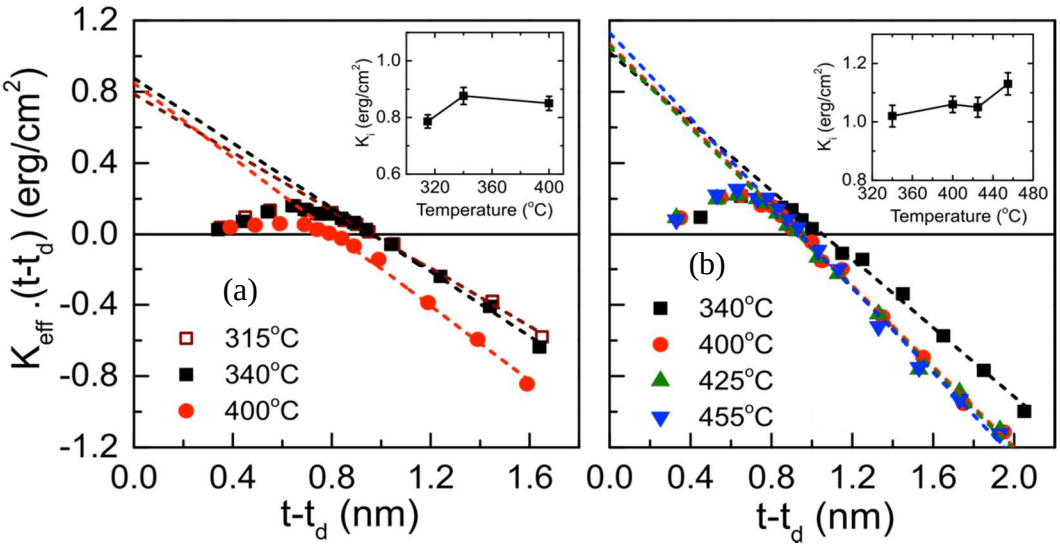

Figure 1: $K_{eff}.(t-t_d)$ vs. $(t-t_d)$ at different annealing temperatures of FeCoB storage electrodes with (a) Ta 1nm and (b) W2/Ta1 nm caps. Corresponding insets are K_i versus annealing temperature plot.

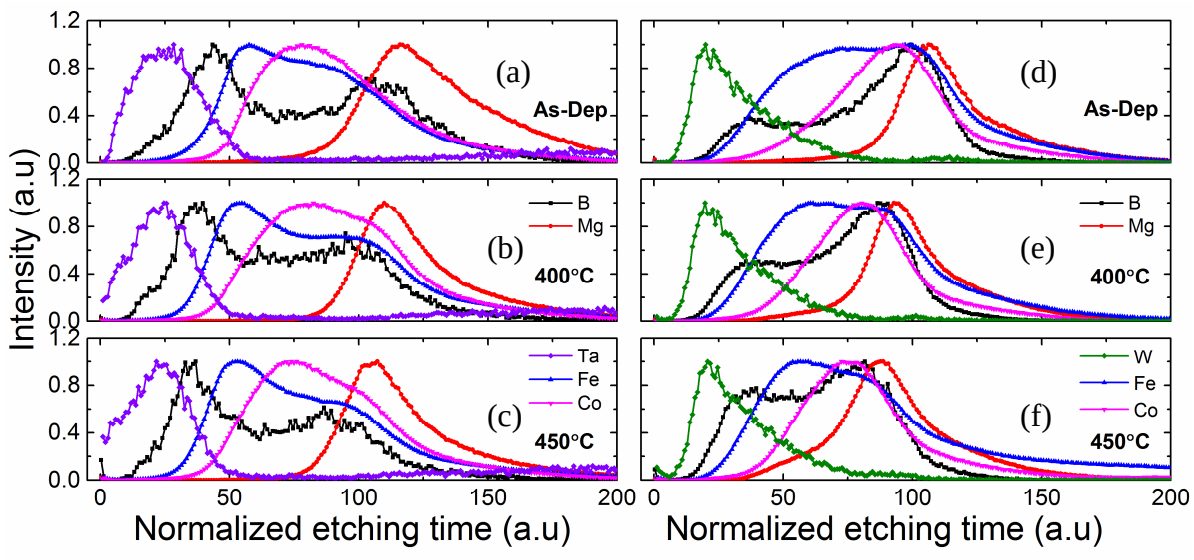

Figure 2: DSIMS depth profile of half-MTJ stacks (Si/MgO ~1/FeCoB 1.6/cap 2/Pt 3 nm) with (a-c) Ta 2 nm cap and (d-f) W 2 nm cap layers after different annealing stages. Color boxes are guide to eye from surface to Si substrate.

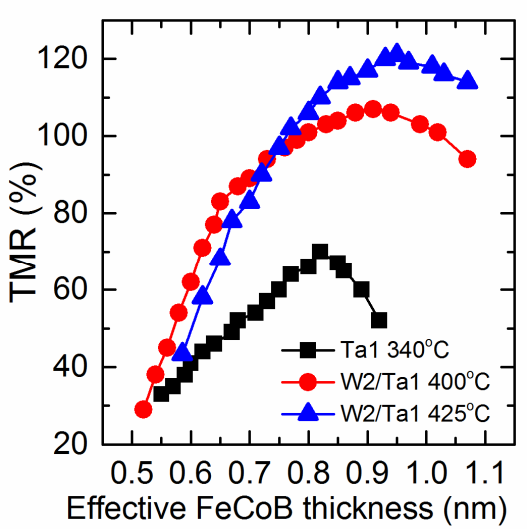

FIG. 3: Tunneling magnetoresistance as a function of effective magnetic thickness of FeCoB storage layer for three pMTJ stacks, one with Ta and another two with W/Ta caps, annealed at different temperatures.

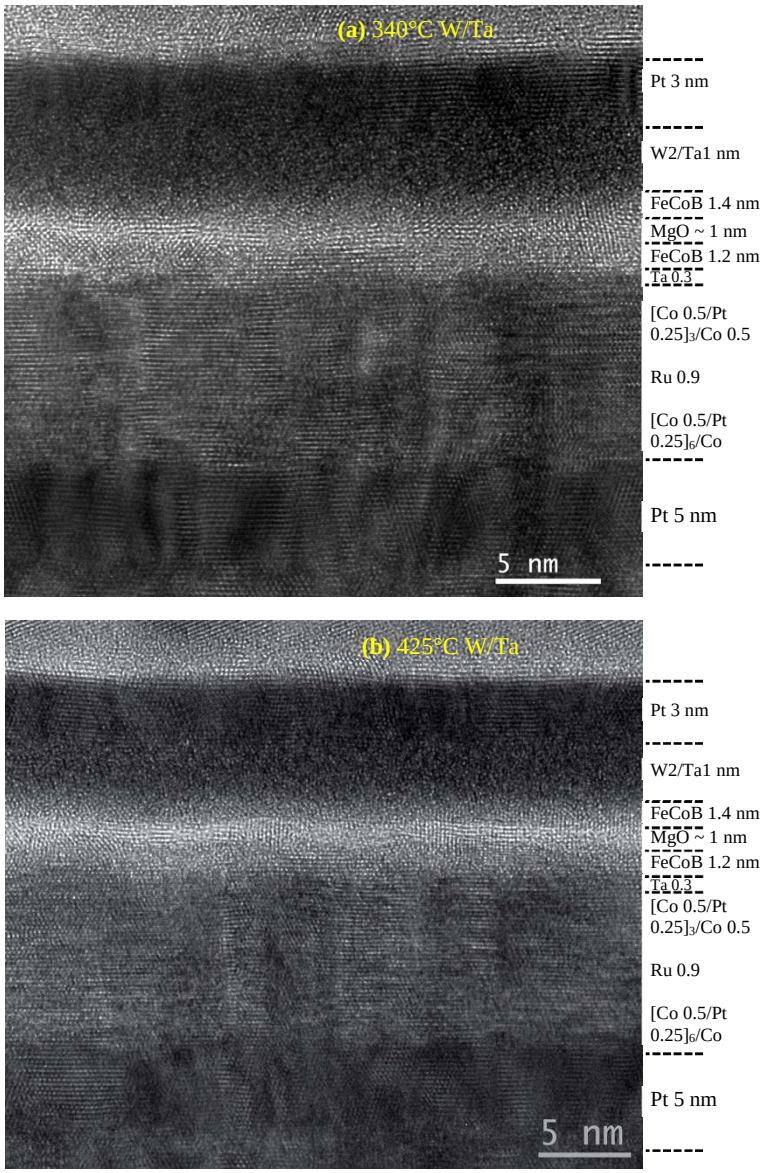

FIG. 4: HRTEM images of pMTJ stacks with W2/Ta1 nm cap after annealing at (a) 340 ℃ and (b) 425 ℃ respectively.

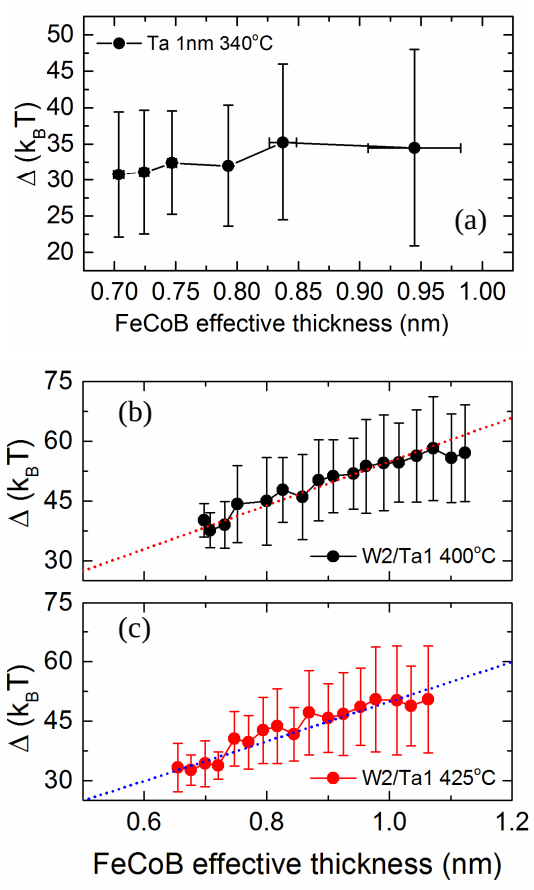

FIG. 5: Thermal stability factor (Δ) of 80 nm memory cells as a function of storage layer thickness for the pMTJ stacks after annealing at 340 ℃, 400 ℃ and 425 ℃ respectively for (a) Ta 1 nm and (b), (c) W2/Ta1 nm cap.